ACS Energy LETTERS

http://pubs.acs.org/journal/aelccp

LETTER

# Role of Tin Chloride in Tin-Rich Mixed-Halide Perovskites Applied as Mesoscopic Solar Cells with a Carbon Counter Electrode

Cheng-Min Tsai,[†] Hui-Ping Wu,[†] Sun-Tang Chang,[‡] Chi-Feng Huang,[†] Chia-Hsin Wang,[‡] Sudhakar Narra,[†] Yaw-Wen Yang,[‡] Chien-Lung Wang,[†] Chen-Hsiung Hung,[§] and Eric Wei-Guang Diau*[,†]

[†]Department of Applied Chemistry and Institute of Molecular Science, National Chiao Tung University, Hsinchu 30010, Taiwan

[‡]National Synchrotron Radiation Research Center, Hsinchu 30076, Taiwan

[§]Institute of Chemistry, Academia Sinica, Taipei 11529, Taiwan

Supporting Information

**ABSTRACT:** We report the synthesis and characterization of alloyed Sn−Pb methylammonium mixed-halide perovskites ($CH_3NH_3Sn_yPb_{1-y}I_{3-x}Cl_x$) to extend light harvesting toward the near-infrared region for carbon-based mesoscopic solar cells free of organic hole-transport layers. The proportions of Sn in perovskites are well-controlled by mixing tin chloride ($SnCl_2$) and lead iodide ($PbI_2$) in varied stoichiometric ratios ($y$ = 0−1). $SnCl_2$ plays a key role in modifying the lattice structure of the perovskite, showing anomalous optical and optoelectronic properties; upon increasing the concentration of $SnCl_2$, the variation of the band gap and band energy differed from those of the $SnI_2$ precursor. The $CH_3NH_3Sn_yPb_{1-y}I_{3-x}Cl_x$ devices showed enhanced photovoltaic performance upon increasing the proportion of $SnCl_2$ until $y$ = 0.75, consistent with the corresponding potential energy levels. The photovoltaic performance was further improved upon adding 30 mol % tin fluoride ($SnF_2$) with device configuration FTO/$TiO_2$/$Al_2O_3$/NiO/C, producing the best power conversion efficiency, 5.13%, with great reproducibility and intrinsic stability.

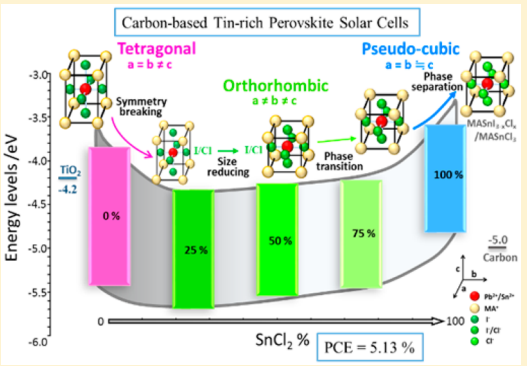


The development of all-solid-state organic−inorganic lead halide perovskite ($CH_3NH_3PbI_3$) solar cells has attracted much attention because of the rapid progress to attain a device performance comparable with that of Si-based solar cells.[1−8] There is, however, an environmental concern regarding toxic element lead inside of the perovskite structure, for which reason lead might be replaced with a nontoxic metallic element such as tin.[9] For this reason, pure tin perovskite ($CH_3NH_3SnI_3$) solar cells have been developed[10−12] with the best device performance attaining a power conversion efficiency (PCE) of ∼6%.[10] One great advantage of a tin perovskite solar cell is its great light-harvesting ability; the absorption spectrum of $CH_3NH_3SnI_3$ exhibits an onset at ∼1000 nm,[11] but the instability of the pure tin perovskite devices under ambient conditions becomes a major challenge to overcome.[10] The instability was speculated to be due to the oxidation of $Sn^{2+}$ to $Sn^{4+}$, causing unfavorable p-type doping during device fabrication.[9−12] To suppress the tin self-doping oxidation and to tune the band gap of the materials, elemental Pb was incorporated in a certain proportion inside of the tin perovskite crystal.[13−15] For example, Hao et al. demonstrated an anomalous behavior of the variation of the band gap in $CH_3NH_3Sn_yPb_{1-y}I_3$ ($y$ = 0−1) with varied tin proportion; the corresponding devices exhibited excellent performance with a PCE over 7% using spiro-OMeTAD as a hole-transporting material (HTM) layer.[13] In contrast, Ogomi et al. showed that devices made of alloyed perovskite $CH_3NH_3Sn_yPb_{1-y}I_3$ did not work with spiro-OMeTAD, but an appreciable efficiency (PCE = 4.18%) was obtained when P3HT was used as a HTM.[14] Jen and co-workers applied mixed Sn−Pb perovskite to a p-type planar heterojunction structure to enhance the crystallinity and surface coverage and attained a PCE of 10.1%.[15] However, only 15% Sn was involved in their perovskite structure, and the device performance degraded dramatically at larger Sn proportions. A stability issue persists for the mixed Sn−Pb perovskite system, in particular, when an organic HTM such as

**Received:** October 8, 2016
**Accepted:** November 1, 2016
**Published:** November 1, 2016





DOI: 10.1021/acsenergylett.6b00514
ACS Energy Lett. 2016, 1, 1086−1093

spiro-OMeTAD containing some reactive additives is employed.[13]

To tackle the stability problem, in the present work, we designed and synthesized alloyed Sn−Pb mixed-halide perovskites ($CH_3NH_3Sn_yPb_{1-y}I_{3-x}Cl_x$) upon dripping the precursor solutions onto the mesoporous films with configuration $TiO_2$/$Al_2O_3$/ to form solar cells free of an organic HTM.[16−19] The device performance and stability were significantly improved when tin precursor $SnI_2$ was replaced with $SnCl_2$. $SnCl_2$ plays a key role to modify the crystal structure of Sn−Pb perovskites, showing disparate trends of band gap narrowing and of the variation of valence band energy levels from those of the $SnI_2$ precursor. The $CH_3NH_3Sn_yPb_{1-y}I_3$ devices made of $SnI_2$ exhibited diminished photovoltaic performance with increasing proportions of $SnI_2$, whereas the $CH_3NH_3Sn_yPb_{1-y}I_{3-x}Cl_x$ devices incorporating $SnCl_2$ displayed enhanced photovoltaic performance with increasing proportions of $SnCl_2$ until $y$ = 0.75, consistent with the potential energy levels determined with ultraviolet photoelectron spectra (UPS). When $SnF_2$ additive[12,20−22] at 30 mol % was added to the $CH_3NH_3Sn_{0.75}Pb_{0.25}I_{3-x}Cl_x$ precursor solution, the device performance improved significantly from PCE = 2.15% (without $SnF_2$) to PCE = 4.35% (with $SnF_2$) with little effect of hysteresis; the short-circuit current density $J_{SC}$ attained a remarkable level, 23.38 ± 0.96 mA $cm^{-2}$, obtained by averaging 36 devices. When a NiO layer was inserted between $Al_2O_3$ and C layers, the performance of a $CH_3NH_3Sn_{0.75}Pb_{0.25}I_{3-x}Cl_x$ device (with $SnF_2$) became further improved to a maximum PCE of 5.13% with an average value of 5.0 ± 0.1% over 17 devices.

The $CH_3NH_3Sn_yPb_{1-y}I_{3-x}Cl_x$ perovskites were synthesized upon mixing $CH_3NH_3I$ (MAI) and $SnCl_2$/$PbI_2$ precursors in equimolar proportions in DMF (Figure 1); the Sn/Pb ratios

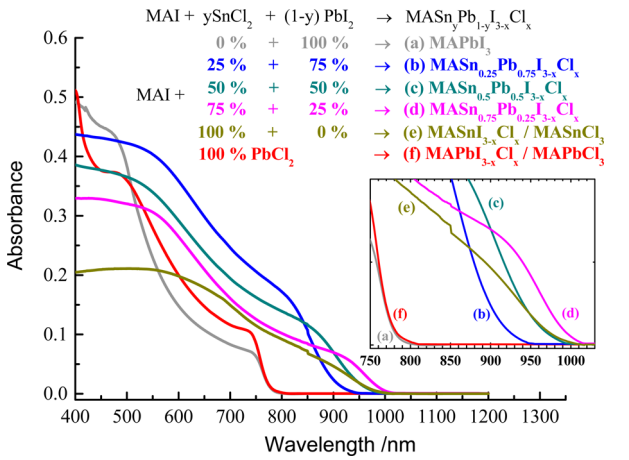


**Figure 1. Absorption spectra of $CH_3NH_3Sn_yPb_{1-y}I_{3-x}Cl_x$ films deposited on glass substrates with Sn/Pb ratios ($y$ = 0−1) controlled by the stoichiometric proportions of the $SnCl_2$/$PbI_2$ precursors summarized at the top. The inset shows enlargement of the spectral tails extending over 1000 nm.**

were controlled upon varying the $SnCl_2$/$PbI_2$ concentrations with molar ratios of 0/100, 25/75, 50/50, 75/25, and 100/0, which correspond to alloy ratios with $y$ = 0, 0.25, 0.5 0.75, and 1, respectively. The SEM/EDS analysis and the XPS spectra, respectively shown in Figures S1 and S2, Supporting Information (SI), confirm that the stoichiometric proportions of the $SnCl_2$/$PbI_2$ (or $SnI_2$/$PbI_2$) mixtures gave the expected Sn/Pb ratios in the perovskites, consistent with those reported elsewhere.[13,14] Figure 1 shows absorption spectra of those alloyed Sn−Pb perovskites deposited on glass substrates. The pure lead perovskites made of 100% $PbI_2$ and 100% $PbCl_2$ are labeled $MAPbI_3$ and $MAPbI_{3-x}Cl_x$, respectively; both spectra showed the same absorption spectral onset at 780 nm (Figure 2). Increasing tin proportions in perovskites shifted the

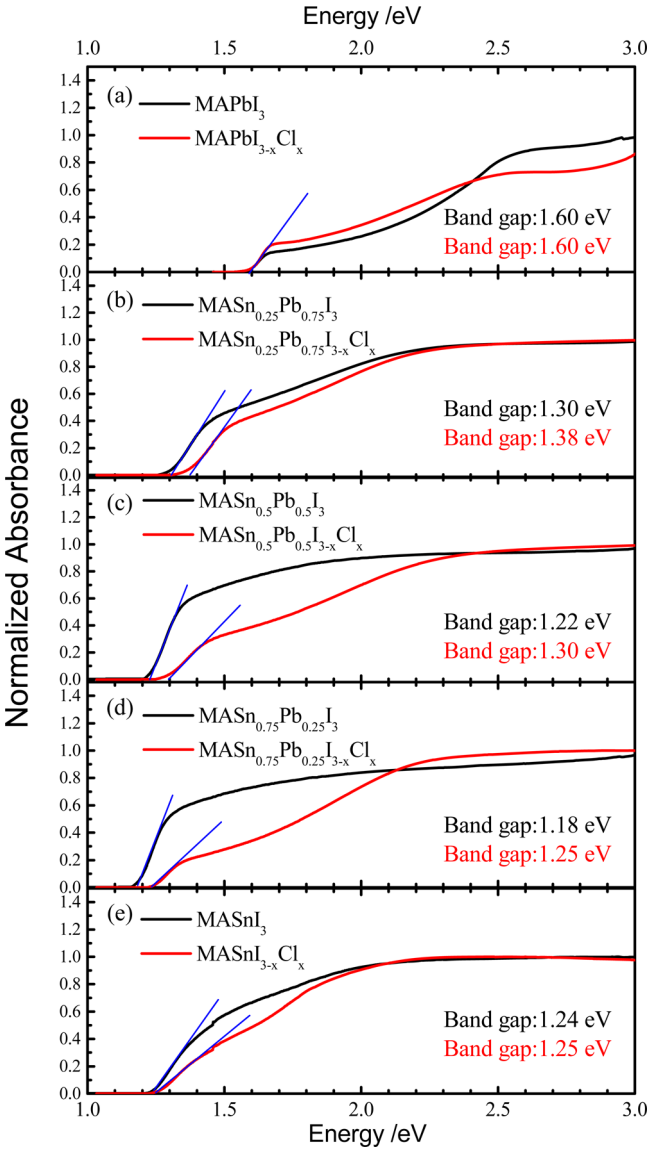


**Figure 2. Normalized absorption spectra of $CH_3NH_3Sn_yPb_{1-y}I_3$ and $CH_3NH_3Sn_yPb_{1-y}I_{3-x}Cl_x$ films deposited on glass substrates with the same Sn/Pb ratios for $y$ = (a) 0, (b) 0.25, (c) 0.5, (d) 0.75, and (e) 1. Blue lines show tangents of the spectra to determine the spectral onsets corresponding to the band gap energies of each species.**

absorption spectra continuously toward longer wavelengths until $y$ = 0.75, whereas pure tin perovskite $MASnI_{3-x}Cl_x$ ($y$ = 1) showed the same spectral shift as that of $y$ = 0.75. Figure 2 compares the band gaps ($E_g$) for the tri-iodide and mixed halide perovskites at varied $SnX_2$/$PbI_2$ (X = Cl or I) proportions. The anomalous band gap behavior reported by Hao et al.[13] for $MASn_yPb_{1-y}I_3$ using stoichiometric $SnI_2$/$PbI_2$ precursors is confirmed in the present work (Figure 2), but in our case, the $MASn_yPb_{1-y}I_{3-x}Cl_x$ perovskites have larger $E_g$ values than their



DOI: 10.1021/acsenergylett.6b00514
ACS Energy Lett. 2016, 1, 1086−1093

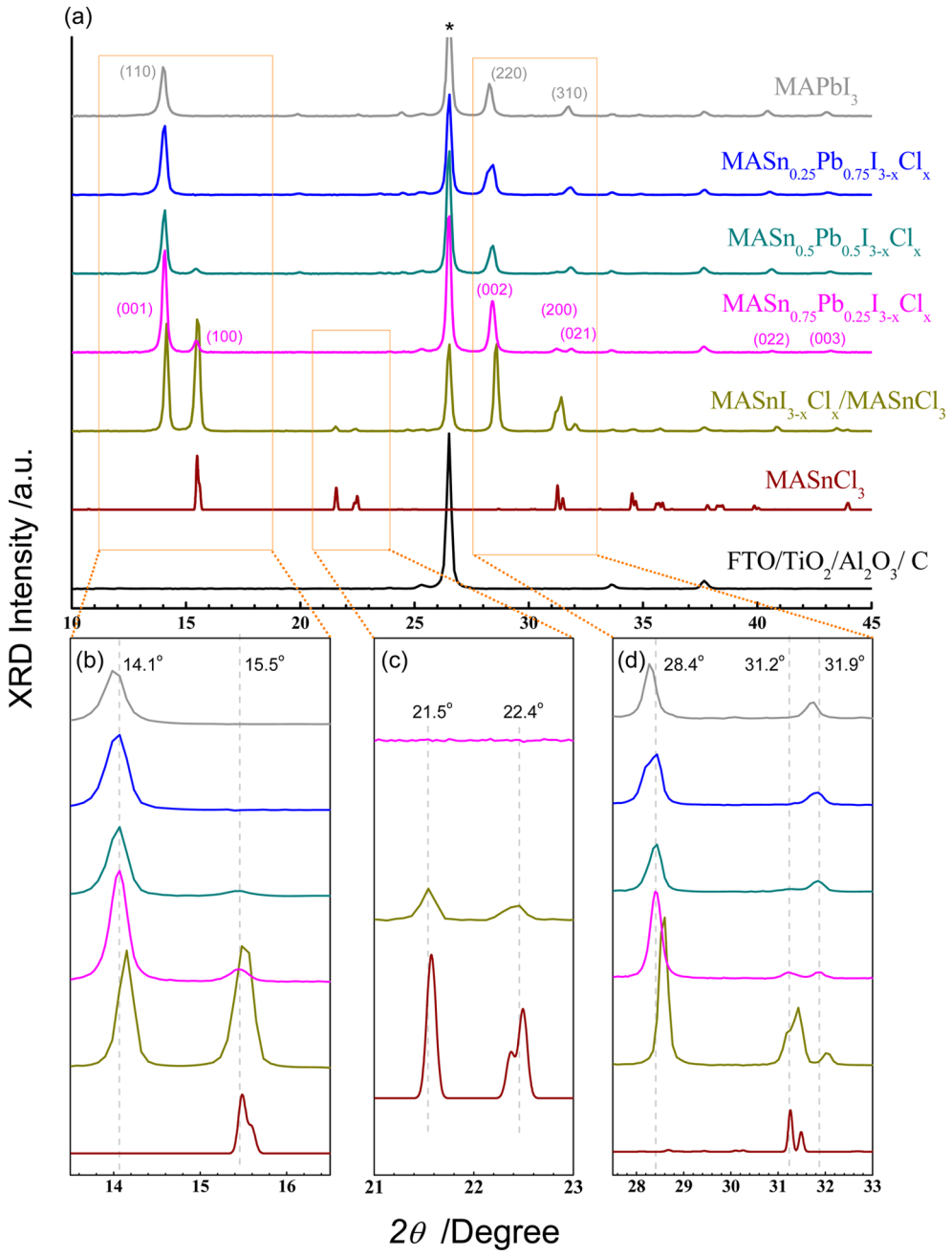


**Figure 3. (a) XRD patterns of $CH_3NH_3Sn_yPb_{1-y}I_{3-x}Cl_x$ films deposited on mesoporous FTO/$TiO_2$/$Al_2O_3$/C substrates with Sn/Pb ratios controlled with varied stoichiometric ratios of $SnCl_2$/$PbI_2$ precursors. The expansions of the characteristic XRD patterns in three diffraction regions highlighted in orange boxes are shown in (b–d). The intense XRD features marked "*" in (a) correspond to the contribution of the carbon layer of the devices. The XRD patterns of the pure phase of $MASnCl_3$ are reproduced from the ICSD database with code number 110664.**

$MASn_yPb_{1-y}I_3$ counterparts for alloyed compositions within $y$ = 0.25–0.75 (Figure 2). The $SnCl_2$ species thus plays a key role to modify the crystal structures for the observed variation of the band gap in the series of perovskite materials.

Figure 3a shows X-ray diffraction (XRD) patterns of $MASn_yPb_{1-y}I_{3-x}Cl_x$ perovskites deposited on FTO/$TiO_2$/$Al_2O_3$/C substrates with $y$ = 0, 0.25, 0.5 0.75, and 1; the corresponding spectral expansions in three specific diffraction regions are shown in Figure 3b–d. The intense XRD features at 26.5° marked "*" arise from a contribution of the carbon layer of the substrates for all devices. To avoid interference of the intense background signals, we performed XRD measurements for both $MASn_yPb_{1-y}I_3$ and $MASn_yPb_{1-y}I_{3-x}Cl_x$ perovskites deposited on FTO/$TiO_2$/$Al_2O_3$ substrates; the corresponding results are shown in Figure S3a,b, SI, respectively.

Our XRD patterns of $MASn_yPb_{1-y}I_3$ are fully consistent with those of Kanatzidis and co-workers,[9,13] showing no contribution from the $(MA)_2SnI_6$ compound characterized with three gray vertical lines shown in Figure S3a, SI; this observation indicates that the p-type self-doping due to the oxidation of $Sn^{2+}$ to form $Sn^{4+}$ in our $MASn_yPb_{1-y}I_3$ system was absent. According to the XRD simulations,[9,13] the $MASn_yPb_{1-y}I_3$ crystals changed from a tetragonal structure at $y$ = 0 ($MAPbI_3$) to a pseudocubic structure at $y$ = 1 ($MASnI_3$)



DOI: 10.1021/acsenergylett.6b00514
ACS Energy Lett. 2016, 1, 1086–1093

through the replacement of Pb with Sn of a smaller size. The transition of the structural change occurred at $y \approx 0.5$; these results were confirmed with our TOPAS analysis (Figure S4 and Table S1, SI). In contrast, upon increasing the $SnCl_2$ proportion, the XRD patterns of $MASn_yPb_{1-y}I_{3-x}Cl_x$ with $y \geq 0.5$ exhibit two additional XRD signals indicated as solid gray lines in Figure S3b, SI; we highlight these two XRD characteristics in panels (b) and (d) of Figure 3, respectively. The extra diffraction signals might be due to a contribution of the pure $MASn_yPb_{1-y}Cl_3$ phase mixed with the $MASn_yPb_{1-y}I_{3-x}Cl_x$ phase,[23,24] but cocrystallization in separate phases should not alter the band gaps of perovskite, as reported by Colella et al.[23] Two separate crystal phases existed for $y = 0$ (100% $PbCl_2$ precursor) and $y = 1$ (100% $SnCl_2$ precursor) because the changes in $E_g$ are negligible for cases with 100% chloride precursors (Figure 2); the XRD signals marked "#" and "*" in Figure S3b, SI, are due to the contributions of $MAPbCl_3$ and $MASnCl_3$, respectively.[23−25]

Chloride is expected to participate in the formation of Cl-containing perovskite crystals to explain the changes of the band gaps for $0.25 \leq y \leq 0.75$ shown in Figure 2, as we explain in what follows for three points. First, as shown in Figure 3b,d, the major XRD signals of perovskites $MASn_yPb_{1-y}I_{3-x}Cl_x$ ($0.25 \leq y \leq 0.75$) at 14.1 and 28.4° correspond to facets (001) and (002) shifted only slightly from signals (110) and (220) of $MAPbI_3$ ($y = 0$), respectively, but those of the $y = 1$ sample showed much greater shifts toward large diffraction angles. Second, the characteristic XRD signals of the $y = 0.75$ sample at 31.2 and 31.9° (Figure 3d) corresponding to facets (200) and (021) differ from those of the $y = 1$ sample. Third, as shown in Figure 3c, the diffraction signals at 21.5 and 22.4° appearing for the $y = 1$ sample (100% $SnCl_2$) can be unambiguously assigned to the contribution of the pure $MASnCl_3$ phase,[25] but this characteristic was not found in samples with $0.25 \leq y \leq 0.75$. The SEM/EDS mapping images shown in Figure S5, SI, indicate that the chlorine elements evenly distributed inside of the perovskite films. Therefore, the XRD signals were simulated using the TOPAS software including the effect of Cl doping for samples $0.25 \leq y \leq 0.75$ deposited on the FTO/$TiO_2$/$Al_2O_3$ substrates; the corresponding results are shown in Figure S6 and Table S2, SI.

Our XRD results indicate that the effect of Cl doping at $y = 0.25$ (25% $SnCl_2$) was significant to shrink the size of the unit cell and change the crystal from the tetragonal structure (symmetry *I*4*cm*) to the orthorhombic structure (symmetry *Iba*2). Compared to the $MASn_yPb_{1-y}I_3$ system with $y = 0.25$ (25% $SnI_2$), the 1% size contraction in the unit cell with reduced symmetry of the space group should be responsible for the change of the band gap (0.08 eV) shown in Figure 2. For Cl doping at $y = 0.5$ (50% $SnCl_2$), the crystal symmetry was reduced to *Pmm*2 for an orthorhombic structure with a substantially smaller unit cell. The size of the orthorhombic lattice further decreased for $y = 0.75$ (75% $SnCl_2$), but the lattice became a pseudocubic structure (symmetry *P*4*mm*) with a larger size for $y = 1$ (100% $SnCl_2$) because the Cl-doped $MASnI_{3-x}Cl_x$ crystal was contaminated with the pure $MASnCl_3$ phase. Differing from the case of triiodide perovskites, incorporation of chloride in $MASn_yPb_{1-y}I_{3-x}Cl_x$ with $y = 0.25−0.75$ broke the symmetry of the space group, with a tendency to decrease the volume of the unit cell until $y = 1.0$ at which phase separation occurred. We thus discovered that increasing the doping levels of chloride in tin-rich alloyed perovskites altered the crystal structure to a decreased symmetry and a smaller unit cell; this structural alteration has an impact on the optical, electronic, and photovoltaic properties of the materials, as we discuss in what follows.

The energy levels of the valence band ($E_{VB}$) of both alloyed perovskite systems were investigated with UPS techniques at an excitation photon energy of 36.4 eV from a synchrotron radiation light source in an ultrahigh vacuum system. The photoelectron kinetic energies and binding energies were determined from the two edges of the UPS spectra to obtain the $E_{VB}$ levels for the $MASn_yPb_{1-y}I_3$ and $MASn_yPb_{1-y}I_{3-x}Cl_x$ systems; the corresponding UPS raw data and analysis are shown in Figures S7 and S8, SI, respectively. The energy levels of the conduction band ($E_{CB}$) were determined from scaling the $E_{VB}$ levels with the corresponding $E_g$ values (Figure 2). Figure 4a,b shows both $E_{VB}$ and $E_{CB}$ energy levels for

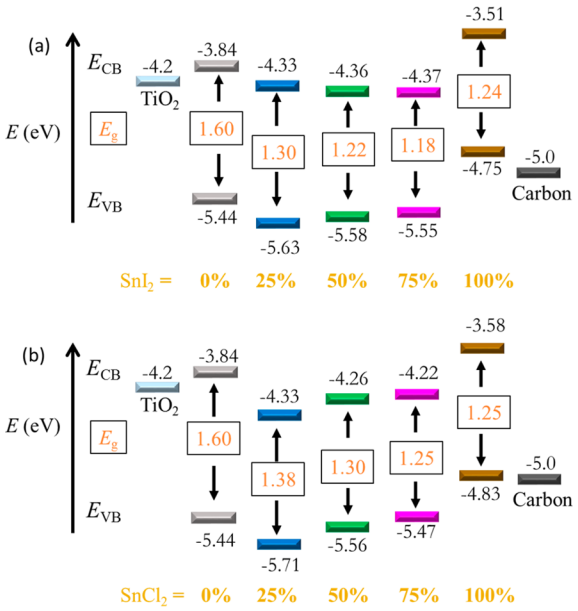


**Figure 4. Potential energy diagrams (energies in eV with respect to vacuum) of (a) $CH_3NH_3Sn_yPb_{1-y}I_3$ and (b) $CH_3NH_3Sn_yPb_{1-y}I_{3-x}Cl_x$ films with Sn/Pb ratios controlled with $SnI_2/PbI_2$ and $SnCl_2/PbI_2$ precursors, respectively, at varied concentrations as indicated. $E_{VB}$ and $E_{CB}$ represent the potential levels of the valence band and conduction band, respectively; $E_g$ represents the energy band gap.**

$MASn_yPb_{1-y}I_3$ and $MASn_yPb_{1-y}I_{3-x}Cl_x$, respectively. For $MASn_yPb_{1-y}I_3$, there is an apparent discrepancy between two reports: Ogomi et al.[13] showed an increasing trend of $E_{VB}$ upon increasing the $y$ values with $E_{VB} = −4.73$ eV for pure tin perovskite ($y = 1$), whereas Hao et al.[13] reported an opposite trend, except that pure tin perovskite showed $E_{VB} = −5.47$ eV. Yokoyama et al.[26] subsequently reported the same $E_{VB}$ value (−4.75 eV) for $MASnI_3$ as that of Ogomi et al.[14] and attributed the smaller value (−5.47 eV) to the contribution of $MA_2SnI_6$ species arising from oxidation of pure tin perovskite during processing. Our UPS results for pure tin perovskite ($y = 1$) agree satisfactorily with those of Ogomi et al.[13] and Yokoyama et al.[26] For mixed Sn−Pb perovskites, we found that incorporating 25% Sn in perovskite led to an increased work function and binding energy (Figure S9, SI), so that the level of $E_{VB}$ at $y = 0.25$ became significantly less than that of pure lead perovskite ($y = 0$). This effect might be due to the characteristics of the Sn−I bond, which is more covalent than



DOI: 10.1021/acsenergylett.6b00514
ACS Energy Lett. 2016, 1, 1086−1093

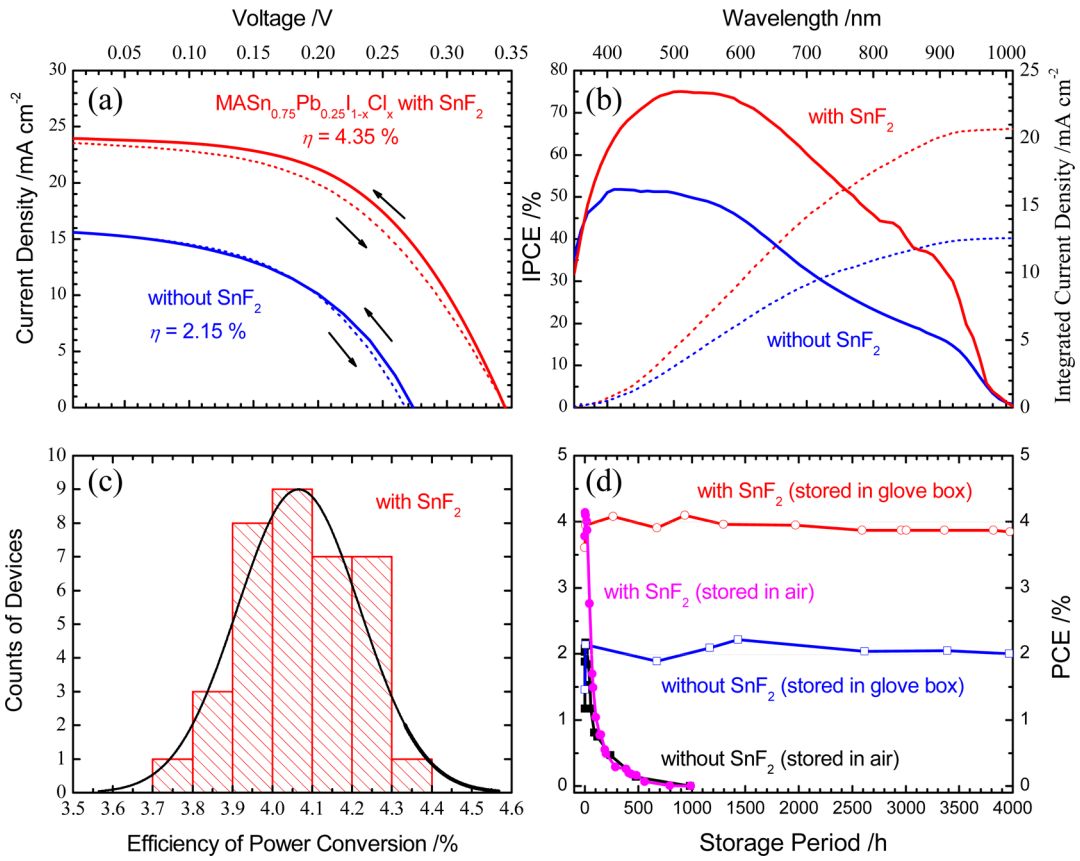


**Figure 5. Photovoltaic performance of $CH_3NH_3Sn_{0.75}Pb_{0.25}I_{3-x}Cl_x$ devices with or without $SnF_2$ additive showing (a) current−voltage curves with reverse (solid) and forward (dashed) scans, (b) IPCE action spectra (solid) and integrated current densities (dashed), (c) a histogram of the PCE with 36 devices fabricated under the same conditions, and (d) efficiency stability profiles as a function of storage period. All of the devices were measured in ambient conditions without encapsulation.**

the Pb−I bond.[26] Upon increasing the ratio of Sn, the work functions slightly increased, but the binding energies decreased nonlinearly to a large extent, as shown in Figure S9, SI. $E_{VB}$ hence shows only a minor increasing trend from $y$ = 0.25 to 0.75 but increases abruptly to −4.75 eV at $y$ = 1 because of the small binding energy (0.25 eV) observed for pure tin perovskite.

For $MASn_yPb_{1-y}I_{3-x}Cl_x$, we again observed a decrease of $E_{VB}$ from $y$ = 0 to 0.25 due to mainly the increased work function (Figure S9b, SI), similar to the case of the triiodide $MASn_yPb_{1-y}I_3$ counterpart, but the increasing trend of $E_{VB}$ from $y$ = 0.25 to 0.75 was more pronounced than that of $MASn_yPb_{1-y}I_3$. For the pure tin mixed-halide perovskite ($y$ = 1), the $E_{VB}$ energy also increased greatly to −4.83 eV, similar to the potential level for that of $MASnI_3$ due to a rapidly decreased binding energy (Figure S9a, SI). Both pure lead perovskite analogues $MAPbI_{3-x}Cl_x$ and $MAPbI_3$ had similar $E_{VB}$ and $E_{CB}$ levels, indicating the involvement of trichloride perovskites in separate phases for pure tin and pure lead mixed-halide perovskites, as discussed previously. The pronounced trend of increasing $E_{VB}$ energy levels of $MASn_yPb_{1-y}I_{3-x}Cl_x$ from $y$ = 0.25 to 0.75 might be due to the enhanced chloride doping levels to modify the crystal structure with a decreased symmetry of the space group that produces a smaller binding energy and a larger kinetic energy than its triiodide $MASn_yPb_{1-y}I_3$ counterpart, as we observed herein (Figures S7−S9, SI). Through a systematic narrowing of the band gaps, the $E_{CB}$ levels of $MASn_yPb_{1-y}I_{3-x}Cl_x$ from $y$ = 0.25 to 0.75 showed only a slightly increasing trend, whereas the $E_{CB}$ levels of $MASn_yPb_{1-y}I_3$ showed a slightly decreasing trend from $y$ = 0.25 to 0.75. Similarly, the appreciable increase of both $E_{VB}$ and $E_{CB}$ levels of $MASnI_{3-x}Cl_x$ ($y$ = 1) was due to the small binding energy (0.24 eV), which might be an intrinsic problem for pure tin perovskites.

The solar cell devices were fabricated with the target perovskites deposited onto carbon-based electrode films;[27] the films have a configuration with three screenprinted layers with mesoporous $TiO_2$, $Al_2O_3$, and carbon layers of thickness 1, 1, and 10 $\mu$m. After infiltration of the perovskite precursor solution onto the mesoporous substrate at 25 °C for 10 min, thermal annealing was performed at 70 °C for 30 min to complete the device fabrication at the desired perovskite composition. The side-view SEM images shown in Figure S10, SI, indicate that compact and dense perovskite crystals were uniformly produced inside of the mesoporous films with effective filling of pores. The current−voltage characteristics of the devices were measured under 1 sun AM 1.5G irradiation, with results shown in Figure S11a,b, SI for $MASn_yPb_{1-y}I_3$ and $MASn_yPb_{1-y}I_{3-x}Cl_x$, respectively; the corresponding photovoltaic parameters are summarized in Tables S3 and S4, SI, respectively.

For $MASn_yPb_{1-y}I_3$, our PV results showed a rapid degradation of performance with an increasing proportion of tin in the perovskite, consistent with the trend of $E_{CB}$ levels that are lower than that of $TiO_2$ ($E_{CB}$ = −4.2 eV).[28] We found no efficiency for the $MASnI_3$ device because the $E_{VB}$ level of



DOI: 10.1021/acsenergylett.6b00514
ACS Energy Lett. 2016, 1, 1086−1093

$MASnI_3$ (−4.75 eV) is higher than the work function of our carbon hole conductor (−5.0 eV); the same phenomenon was mentioned by Ogomi et al. using spiro-OMeTAD as the HTM ($E_{HOMO}$ = −5.2 eV).[14] To match the HOMO energy level of the HTM with the $E_{VB}$ level of $MASnI_3$, Ogomi et al.[14] used P3HT as the HTM to obtain an appreciable device performance for the $MASn_{0.5}Pb_{0.5}I_3$ device, attaining a PCE of 4.18%. In contrast, Snaith and co-workers[10] reported an efficiency of 6.4% for the $MASnI_3$ device using a $TiO_2$ electrode, although poor reproducibility of the device performance was found. Hao et al. showed that the $MASnI_3$ device free of a HTM attained a PCE of 3.15%;[12] the device performance increased to PCE = 5.23%[11] and to 5.44%[13] using spiro-OMeTAD as the HTM, in conflict with the results reported by Ogomi et al.[14] Yokoyama et al.[26] reported using a low-temperature vapor-assisted solution process to prepare uniform $MASnI_3$ films; the device performance attained only 1.86%, whereas use of the traditional one-step method led to the $MASnI_3$ devices showing poor performance.

We found that the performance of the $MASn_yPb_{1-y}I_{3-x}Cl_x$ devices showed a different trend: the efficiency was poor at $y$ = 0.25 but increased greatly to attain PCE = 2.15% at $y$ = 0.75; the performance deteriorated again at $y$ = 1 for the pure tin perovskite solar cell. The variation of these efficiencies shows a trend similar to the variation of energy levels shown in Figure 4b, indicating that potential matching is an important factor to promote the device performance for carbon-based HTM-free tin-rich perovskite solar cells. The $E_{CB}$ energy levels of $MASn_yPb_{1-y}I_{3-x}Cl_x$ can be tuned to match the $E_{CB}$ level of $TiO_2$ upon increasing the chloride doping levels; an optimal condition was found to occur at $y$ = 0.75 with a suitable band gap of $E_g$ = 1.25 eV. Because the PL lifetime of tin perovskite was short (<200 ps for $MASnI_3$),[10] charge separation must readily occur either from the interface between the perovskite and $TiO_2$ or from the interface between the perovskite and the carbon electrode. Snaith and co-workers showed negligible efficiencies for pure tin perovskites deposited on a mesoporous $Al_2O_3$ scaffold layer,[10] implying that electron injection from $E_{CB}$ of the perovskite into the $E_{CB}$ level of $TiO_2$ might play an important role for effective charge separation. In our case, the device performance of perovskites in the two series is well explained with the corresponding variations of $E_{CB}$ with respect to that of $TiO_2$, confirming the significance of potential matching in our tin-rich perovskite system.

Even though tin perovskites exhibit suitable band gaps to harvest sunlight toward 1000 nm, their device performances were much worse than those of their lead perovskite counterparts because of the metallic nature of the materials involving tin cationic vacancies. An investigation of $CsSnI_3$ perovskite showed that addition of tin fluoride ($SnF_2$) had the effect of decreasing the concentration of Sn vacancies and thus improving greatly the photovoltaic performance.[20−22] Accordingly, we examined the effect of $SnF_2$ on devices made of alloyed perovskite $MASn_{0.75}Pb_{0.25}I_{3-x}Cl_x$, which exhibited the best performance among the series. Figure S12, SI, shows $J$−$V$ curves of these perovskite devices upon addition of $SnF_2$ with molar ratios $[SnF_2]/[MAI]$ = 0, 10, 20, 30, and 40 mol %; the corresponding photovoltaic parameters are shown in Table S5, SI. The results indicate that the efficiencies systematically increase with increasing concentration of $SnF_2$; the maximum device performance was obtained at a concentration of 30 mol % $SnF_2$, consistent with the $CsSnI_3$ results showing a similar trend.[21]

Figure 5a,b shows $J$−$V$ curves and the corresponding IPCE action spectra, respectively, for the best $MASn_{0.75}Pb_{0.25}I_{3-x}Cl_x$ devices with (30 mol %) and without addition of $SnF_2$. We found that the presence of $SnF_2$ additive was effective to enhance both $J_{SC}$ and $V_{OC}$ values, with the best cell showing $J_{SC}$ = 24.35 mA cm$^{-2}$, $V_{OC}$ = 347 mV, FF = 0.515, and overall efficiency $\eta$ = 4.35%. Integration of the IPCE spectra with a standard AM 1.5G solar photon flux distribution produced photocurrents consistent with those of the $J$−$V$ measurements. We highlight here the great light-harvesting ability of our tin-rich mixed-halide perovskite devices giving a large $J_{SC}$ value: the IPCE spectrum attained a maximum value 75% in the region of 500−550 nm; the efficiencies continued to decrease toward longer wavelengths with an onset near 1000 nm, consistent with the corresponding absorption spectrum shown in Figure 1 and the results of Kumar et al.[21] based on a $SnF_2$−$CsSnI_3$ device. This IPCE spectral feature is consistent with that of Ogomi et al.[14] and that of Yokoyama et al.[26] but contradicts those of Hao et al.[11,13] showing maximum IPCE responses of pure tin and mixed Sn−Pb devices in the near-IR region. The $V_{OC}$ values of our tin-rich perovskites are small compared with those of normal lead perovskites, likely because of the intrinsic defects in tin perovskites. Adding $SnF_2$ decreased the tin vacancies and metallic conductivity to some extent, but trap-assisted recombination might still play a role for the decreased open-circuit voltages observed in our tin-rich perovskite system. Nevertheless, the devices showed a minor effect of hysteresis upon $J$−$V$ scans from both reverse and forward directions, which is an interesting feature for a mesoscopic perovskite solar cell.[29]

Thirty-six identical devices were fabricated under the same experimental conditions; the corresponding photovoltaic data are summarized in Tables S6, SI. The average photovoltaic parameters of devices with $SnF_2$ (30 mol %) additive are $J_{SC}$ = 23.38 ± 0.96 mA cm$^{-2}$, $V_{OC}$ = 340 ± 14 mV, FF 0.512 ± 0.021, and PCE = 4.06 ± 0.15%. A histogram of PCE in Figure 5c indicates a narrow distribution of the photovoltaic performance, spanning the range of 3.71−4.35%. Snaith and co-workers[10] showed a broad distribution of PCE; their data ranged from 0 to 6% but with over 80% of the data spread in the range of 0−3%. We tested the stability of the thin-film samples in ambient air conditions with perovskites fabricated with $SnI_2$ and $SnCl_2$ precursors in varied proportions; the results are shown in Figure S13, SI. We thus demonstrated the great reproducibility and stability of the tin-rich perovskite devices fabricated using the $SnCl_2$ precursor beyond those properties of the $MASnI_3$ devices with the $SnI_2$ precursor. As shown in Figure 5d, the performance of the $MASn_{0.75}Pb_{0.25}I_{3-x}Cl_x$ device degraded in ambient air rapidly to near-background level after 500 h, but the devices were stable when stored in a $N_2$-filled glovebox for over 4000 h.

To improve further the overall photovoltaic performance of the $CH_3NH_3Sn_{0.75}Pb_{0.25}I_{3-x}Cl_x$ devices, we added a layer of nickel oxide between $Al_2O_3$ and the carbon electrode so that the NiO layer served as a hole-extraction medium to improve $V_{OC}$ of the device. The thickness of the NiO layer was varied from 250 to 1000 nm; the corresponding photovoltaic performances are shown in Figure S14 and Table S7, SI. The additional NiO layer slightly decreased $J_{SC}$ but enhanced $V_{OC}$ to a large extent at a thickness of the NiO film greater than ∼500 nm. The photovoltaic performance of the NiO device was optimized at a film thickness of 750 nm, showing $J_{SC}$ = 19.63 mA cm$^{-2}$, $V_{OC}$ = 457 mV, and FF = 0.572, corresponding to an



DOI: 10.1021/acsenergylett.6b00514
ACS Energy Lett. 2016, 1, 1086−1093

overall PCE of 5.13%. Seventeen identical tin-rich perovskite devices were fabricated with film configuration FTO/$TiO_2$/$Al_2O_3$/NiO/C under the same experimental conditions. The corresponding histogram of PCE is shown in Figure S15, SI, which gives an average PCE of 5.0 ± 0.1% with $J_{SC}$ = 18.93 ± 1.07 mA $cm^{-2}$, $V_{OC}$ = 462 ± 15 mV, and FF = 0.570 ± 0.019.

In conclusion, we developed alloyed Sn−Pb mixed-halide perovskites in a new series, $MASn_yPb_{1-y}I_{3-x}Cl_x$, using precursor solutions containing methylammonium iodide and metal halide mixtures in varied stoichiometric ratios. The Sn/Pb ratios in the perovskites were controlled upon mixing the $SnCl_2$/$PbI_2$ precursors in molar ratios of 0/100, 25/75, 50/50, 75/25, and 100/0. Differing from its $SnI_2$ analogue, $SnCl_2$ had an effect to participate in the crystallization of perovskite at increased concentrations to modify the crystal structures and to alter the optical and electronic properties of the materials. We found anomalous variations of band gaps and band energies for these perovskites; that with $y$ = 0.75 gave the best potential matching for electron transport in $TiO_2$ and for hole transport in the carbon electrode. The best photovoltaic performance was also found at this composition. When $SnF_2$ (30 mol %) was incorporated as an additive to decrease the intrinsic defects of this tin-rich mixed-halide perovskite, the short-circuit photocurrent density of the device was significantly improved to an extraordinary level with an average $J_{SC}$ = 23.38 ± 0.96 mA $cm^{-2}$. The fluctuation of the photovoltaic performance was small, which represents excellent reproducibility and stability of the devices under investigation. Moreover, the $V_{OC}$ of the $MASn_{0.75}Pb_{0.25}I_{3-x}Cl_x$ devices was further improved upon adding a layer of NiO, attaining the best device performance PCE of 5.13%. The present work thus opens a new door for further development of lead-free perovskite solar cells with superior stability and improved performance.

## ■ ASSOCIATED CONTENT

### Supporting Information

The Supporting Information is available free of charge on the ACS Publications website at DOI: 10.1021/acsenergylett.6b00514.

Experimental section, lattice parameters of various conditions, photovoltaic parameters of various devices, SEM/EDS figure, XPS of various conditions, XRD of various conditions, TOPAS simulation of various conditions, UPS of various conditions, SEM side-view images, current−voltage characteristics of various devices, current−voltage and IPCE curves of $CH_3NH_3Sn_{0.75}Pb_{0.25}I_{3-x}Cl_x$ devices, stability tests of $CH_3NH_3Sn_yPb_{1-y}I_3$ and $CH_3NH_3Sn_yPb_{1-y}I_{3-x}Cl_x$ thin-film samples, and histograms of $CH_3NH_3Sn_{0.75}Pb_{0.25}I_{3-x}Cl_x$ devices (PDF)

## ■ AUTHOR INFORMATION


### Corresponding Author

*E-mail: diau@mail.nctu.edu.tw.


### Notes

The authors declare no competing financial interest.

## ■ ACKNOWLEDGMENTS

We thank the National Synchrotron Radiation Research Center (NSRRC), Hsinchu, Taiwan, for provision of beam time for UPS and XPS measurements. The Ministry of Science and Technology (MOST) of Taiwan supported this work with Contracts MOST 105-2119-M-009-011-MY3 and MOST 105-2119-M-009-001.

## ■ REFERENCES


(1) Kim, H. S.; Lee, C. R.; Im, J. H.; Lee, K. B.; Moehl, T.; Marchioro, A.; Moon, S. J.; Humphry-Baker, R.; Yum, J. H.; Moser, J. E.; et al. Lead Iodide Perovskite Sensitized All-Solid-State Submicron Thin Film Mesoscopic Solar Cell with Efficiency Exceeding 9%. *Sci. Rep.* **2012**, *2*, 591.

(2) Lee, M. M.; Teuscher, J.; Miyasaka, T.; Murakami, T. N.; Snaith, H. J. Efficient Hybrid Solar Cells Based on Meso-Superstructured Organometal Halide Perovskites. *Science* **2012**, *338*, 643−647.

(3) Rhee, J. H.; Chung, C.-C.; Diau, E. W.-G. A Perspective of Mesoscopic Solar Cells Based on Metal Chalcogenide Quantum Dots and Organometal-Halide Perovskites. *NPG Asia Mater.* **2013**, *5*, e68.

(4) Liu, M.; Johnston, M. B.; Snaith, H. J. Efficient Planar Heterojunction Perovskite Solar Cells by Vapour Deposition. *Nature* **2013**, *501*, 395−398.

(5) Zhou, H.; Chen, Q.; Li, G.; Luo, S.; Song, T.-b.; Duan, H.-S.; Hong, Z.; You, J.; Liu, Y.; Yang, Y. Interface Engineering of Highly Efficient Perovskite Solar Cells. *Science* **2014**, *345*, 542−546.

(6) Gao, P.; Grätzel, M.; Nazeeruddin, M. K. Organohalide Lead Perovskites for Photovoltaic Applications. *Energy Environ. Sci.* **2014**, *7*, 2448−2463.

(7) Yang, W. S.; Noh, J. H.; Jeon, N. J.; Kim, Y. C.; Ryu, S.; Seo, J.; Seok, S. I. High-Performance Photovoltaic Perovskite Layers Fabricated through Intramolecular Exchange. *Science* **2015**, *348*, 1234−1237.

(8) Zhou, Z.; Pang, S.; Liu, Z.; Xu, H.; Cui, G. Interface Engineering for High-Performance Perovskite Hybrid Solar Cells. *J. Mater. Chem. A* **2015**, *3*, 19205−19217.

(9) Stoumpos, C. C.; Malliakas, C. D.; Kanatzidis, M. G. Semiconducting Tin and Lead Iodide Perovskites with Organic Cations: Phase Transitions, High Mobilities, and Near-Infrared Photoluminescent Properties. *Inorg. Chem.* **2013**, *52*, 9019−9038.

(10) Noel, N. K.; Stranks, S. D.; Abate, A.; Wehrenfennig, C.; Guarnera, S.; Haghighirad, A.-A.; Sadhanala, A.; Eperon, G. E.; Pathak, S. K.; Johnston, M. B.; et al. Lead-Free Organic−Inorganic Tin Halide Perovskites for Photovoltaic Applications. *Energy Environ. Sci.* **2014**, *7*, 3061−3068.

(11) Hao, F.; Stoumpos, C. C.; Cao, D. H.; Chang, R. P. H.; Kanatzidis, M. G. Lead-Free Solid-State Organic−Inorganic Halide Perovskite Solar Cells. *Nat. Photonics* **2014**, *8*, 489−494.

(12) Hao, F.; Stoumpos, C. C.; Guo, P.; Zhou, N.; Marks, T. J.; Chang, R. P. H.; Kanatzidis, M. G. Solvent-Mediated Crystallization of $CH_3NH_3SnI_3$ films for Heterojunction Depleted Perovskite Solar Cells. *J. Am. Chem. Soc.* **2015**, *137*, 11445−11452.

(13) Hao, F.; Stoumpos, C. C.; Chang, R. P.; Kanatzidis, M. G. Anomalous Band Gap Behavior in Mixed Sn and Pb Perovskites Enables Broadening of Absorption Spectrum in Solar Cells. *J. Am. Chem. Soc.* **2014**, *136*, 8094−8099.

(14) Ogomi, Y.; Morita, A.; Tsukamoto, S.; Saitho, T.; Fujikawa, N.; Shen, Q.; Toyoda, T.; Yoshino, K.; Pandey, S. S.; Ma, T.; et al. $CH_3NH_3Sn_xPb_{(1-x)}I_3$ Perovskite Solar Cells Covering up to 1060 nm. *J. Phys. Chem. Lett.* **2014**, *5*, 1004−1011.

(15) Zuo, F.; Williams, S. T.; Liang, P. W.; Chueh, C. C.; Liao, C. Y.; Jen, A. K. Binary-Metal Perovskites toward High-Performance Planar-Heterojunction Hybrid Solar Cells. *Adv. Mater.* **2014**, *26*, 6454−6460.

(16) Ku, Z.; Rong, Y.; Xu, M.; Liu, T.; Han, H. Full Printable Processed Mesoscopic $CH_3NH_3PbI_3$/$TiO_2$ Heterojunction Solar Cells with Carbon Counter Electrode. *Sci. Rep.* **2013**, *3*, 3132.

(17) Mei, A.; Li, X.; Liu, L.; Ku, Z.; Liu, T.; Rong, Y.; Xu, M.; Hu, M.; Chen, J.; Yang, Y.; et al. A Hole-Conductor-Free, Fully Printable Mesoscopic Perovskite Solar Cell with High Stability. *Science* **2014**, *345*, 295−298.

(18) Cao, K.; Cui, J.; Zhang, H.; Li, H.; Song, J.; Shen, Y.; Cheng, Y.; Wang, M. Efficient Mesoscopic Perovskite Solar Cells Based on the $CH_3NH_3PbI_2Br$ Light Absorber. *J. Mater. Chem. A* **2015**, *3*, 9116−9122.




DOI: 10.1021/acsenergylett.6b00514
*ACS Energy Lett.* 2016, 1, 1086−1093

(19) Kojima, A.; Teshima, K.; Shirai, Y.; Miyasaka, T. Organometal Halide Perovskites as Visible-Light Sensitizers for Photovoltaic Cells. *J. Am. Chem. Soc.* **2009**, *131*, 6050−6051.
(20) Chung, I.; Lee, B.; He, J.; Chang, R. P.; Kanatzidis, M. G. All-Solid-State Dye-Sensitized Solar Cells with High Efficiency. *Nature* **2012**, *485*, 486−489.
(21) Kumar, M. H.; Dharani, S.; Leong, W. L.; Boix, P. P.; Prabhakar, R. R.; Baikie, T.; Shi, C.; Ding, H.; Ramesh, R.; Asta, M.; et al. Lead-Free Halide Perovskite Solar Cells with High Photocurrents Realized through Vacancy Modulation. *Adv. Mater.* **2014**, *26*, 7122−7127.
(22) Sabba, D.; Mulmudi, H. K.; Prabhakar, R. R.; Krishnamoorthy, T.; Baikie, T.; Boix, P. P.; Mhaisalkar, S.; Mathews, N. Impact of Anionic Br−Substitution on Open Circuit Voltage in Lead Free Perovskite ($CsSnI_{3-x}Br_x$) Solar Cells. *J. Phys. Chem. C* **2015**, *119*, 1763−1767.
(23) Colella, S.; Mosconi, E.; Fedeli, P.; Listorti, A.; Gazza, F.; Orlandi, F.; Ferro, P.; Besagni, T.; Rizzo, A.; Calestani, G.; et al. $MAPbI_{3-x}Cl_x$ mixed Halide Perovskite for Hybrid Solar Cells: The Role of Chloride as Dopant on the Transport and Structural Properties. *Chem. Mater.* **2013**, *25*, 4613−4618.
(24) Prajongtat, P.; Dittrich, T. Precipitation of $CH_3NH_3PbCl_3$ in $CH_3NH_3PbI_3$ and Its Impact on Modulated Charge Separation. *J. Phys. Chem. C* **2015**, *119*, 9926−9933.
(25) Yamada, K.; Nakada, K.; Takeuchi, Y.; Nawa, K.; Yamane, Y. Tunable Perovskite Semiconductor $CH_3NH_3Sn_{x3}$ (x: Cl, Br, or I) Characterized by X-Ray and Dta. *Bull. Chem. Soc. Jpn.* **2011**, *84*, 926−932.
(26) Yokoyama, T.; Cao, D. H.; Stoumpos, C. C.; Song, T. B.; Sato, Y.; Aramaki, S.; Kanatzidis, M. G. Overcoming Short-Circuit in Lead-Free $CH_3NH_3SnI_3$ Perovskite Solar Cells Via Kinetically Controlled Gas-Solid Reaction Film Fabrication Process. *J. Phys. Chem. Lett.* **2016**, *7*, 776−782.
(27) Chan, C.-Y.; Wang, Y.; Wu, G.-W.; Diau, E. W.-G. Solvent-Extraction Crystal Growth for Highly Efficient Carbon-Based Mesoscopic Perovskite Solar Cells Free of Hole Conductors. *J. Mater. Chem. A* **2016**, *4*, 3872−3878.
(28) Cao, G. *Annual Review of Nano Research*; World Scientific Publishing Company Pte Limited, 2009.
(29) Snaith, H. J.; Abate, A.; Ball, J. M.; Eperon, G. E.; Leijtens, T.; Noel, N. K.; Stranks, S. D.; Wang, J. T.-W.; Wojciechowski, K.; Zhang, W. Anomalous Hysteresis in Perovskite Solar Cells. *J. Phys. Chem. Lett.* **2014**, *5*, 1511−1515.



DOI: 10.1021/acsenergylett.6b00514
*ACS Energy Lett.* 2016, 1, 1086−1093